Photoexcitation of electronic instabilities in one-dimensional charge-transfer systems

Julián Rincón,[1] K. A. Al-Hassanieh,[1] Adrian E. Feiguin,[2] and Elbio Dagotto[3,4]

[1] *Center for Nanophase Materials Sciences, Oak Ridge National Laboratory, Oak Ridge, Tennessee 37831, USA*
[2] *Department of Physics, Northeastern University, Boston, Massachusetts 02115, USA*
[3] *Department of Physics and Astronomy, The University of Tennessee, Knoxville, Tennessee 37996, USA*
[4] *Materials Science and Technology Division, Oak Ridge National Laboratory, Oak Ridge, Tennessee 37831, USA*

(Dated: October 21, 2014)

We investigate the real-time dynamics of photoexcited electronic instabilities in a charge-transfer system model, using the time-dependent density matrix renormalization group method. The model of choice was the quarter-filled one-dimensional extended Peierls-Hubbard Hamiltonian interacting with classical few-cycle electromagnetic radiation. The results show that only one electronic instability drives the main features of the photogenerated time-dependent behavior. Indeed, the photoresponse of the system shows a large enhancement of the $4k_F$ (bond and charge) instability whereas the $2k_F$ state remains largely unaffected. This conclusion holds regardless of the nature of the optical excitations and whether the system is perturbed resonantly or not. Our results suggest potential applications of charge-transfer systems with slow phononic dynamics as optoelectronic switching devices.

PACS numbers: 78.20.Bh, 78.47.jh, 78.47.J-, 87.15.ht

arXiv:1406.6893v2 [cond-mat.str-el] 18 Oct 2014

I. INTRODUCTION

Accomplishing control over ultrafast and intense light pulses is at the heart of attosecond and femtosecond spectroscopy[1,2]. Applications include subfemtosecond emission of extreme ultraviolet radiation, molecular dissociation, and the manipulation of changes in the structure of molecular, atomic, and solid state matter, just to mention a few[1,3,4]. Manipulating such properties of materials via light has opened a realistic and reliable route to the possibility of studying selected emergent states in complex systems such as superconductors, organic charge-transfer solids, Mott and charge density wave insulators, and others[3,4]. Using resonant and intense nonresonant ultrafast pulses of electromagnetic radiation, remarkable experimental outcomes have been observed. Excellent examples include: photoinduced phase transitions, real-space scanning of molecular orbitals, control over dissociation of molecules, study of ionic and electronic motion, melting of ordered states like in superconductors, as well as the analysis of magnetic and charge order[1,3,4].

In the context of nonequilibrium properties, ultrafast optical pulses have allowed the excitation of electrons well above any intrinsic characteristic energy scale or manipulation of the degree of competition between different orders, since usually there is a complex interplay and exchange of energy between different many-body states of the system's Hilbert space. By probing the system's dynamics by shaking it with a pulse of light, it is possible to access states present in the energy spectrum which are not accessible via experiments carried out by changing the temperature[3,5,6]. These types of *nonthermal states* often contain coexisting orders that are not usually present in the standard ground or thermal states, making a remarkable difference in the way the system evolves after photoexcitation. Experimental access to these highly nontrivial states has been accomplished in a variety of systems, as discussed above.

Quantum materials, also known as strongly correlated systems[3], belong to a family of systems where several phases compete producing extremely complex many-body states. Although a single phase may dominate the ground state, competing instabilities are often hidden at higher energies, which can be accessible with intense ultrafast pulses of light. The electromagnetic radiation will reshape the energy distribution of the many-body spectrum, reordering the relevance of the states, and in the case of a time-dependent electric field, switching rapidly from one to another[3,4].

When quantum materials are pumped with ultrafast light pulses, interesting dynamics ensues between several electronic instabilities such as charge order (CO), charge density waves (CDWs), spin density waves (SDWs), spin-Peierls (SP) states, bond order waves (BOWs), and others[3]. Representative materials that display several of these instabilities are the so-called charge-transfer salts: $(TM)X_2$, where TM is either TMTSF (tetramethytetraselenafulvalene) or TMTTF (tetramethyltetrathiafulvalene) while X_2 can be ClO_4, PF_6, or Br[7]. These compounds have in common that the filling factor can be considered as quarter-filled, in terms of either electrons or holes, and effectively they behave as one-dimensional (1D) chains. Typical instabilities found in these molecular systems are $2k_F$ and $4k_F$ BOW, CDW, CO, and SP states (k_F is the Fermi wavevector). Also important is the relative phase between the $2k_F$ and $4k_F$ instabilities which will define different ordered states (see Sec. III).

Using pump and probe ultrafast spectroscopy in the organic salt $(EDO\text{-}TTF)_2PF_6$, studies of the photoresponse of the optical conductivity, $\sigma(\omega)$, have reported a phase transition between two different CO states with a gigantic response in $\sigma(\omega)$[5,6]. It was also shown that the photoinduced ordered state could not be assigned to any of the states of the thermal equilibrium spectrum,

but rather to a nonthermal state[5,6]. Similar experimental pump-and-probe studies of the photoexcited charge dynamics have been carried out on similar organic compounds[8].

Theoretical investigations of the photogenerated dynamics of organic compounds have also been reported[9–18]. Using a time-dependent Lanczos approach, the dynamics of $(EDO\text{-}TTF)_2PF_6$ induced by a time-dependent multi cycle electrical field studied the efficiency of the partial melting of the $2k_F$ CO ground state in the presence of different lattice potentials[12]. That work used a quarter-filled 1D Hubbard model with Peierls and Holstein type of electron-phonon couplings, where the vibrational degrees of freedom were treated classically[12]. Another related work, on a similar model and using the same numerical method, observed a complete melting of the CO, where the excess of energy associated with the order was transferred to the generation of phonons[14]. After this process, a complete nonadiabatic decoupling between vibrational and electronic degrees of freedom was reported[14]. Similar results for the half-filled case were reported elsewhere[18].

In this publication, we present a detailed density-matrix renormalization-group (DMRG)[19–21] study of the effect of few-cycle light pulses on the competition between charge and bond instabilities, present in organic compounds, in the pump-and-probe situation. We resort to a quarter-filled 1D extended Peierls-Hubbard Hamiltonian to model the molecular compounds interacting with the incident radiation. This model mimics the setup used in ultrafast spectroscopy measurements, where a portion of the material is pumped with an ultrafast light pulse, lasting typically a few femtoseconds. Here, we focus on the photoresponse of the charge and bond instabilities, and how the system reacts to the interaction with both resonant and nonresonant electric field. Moreover, we also explore all the possible optical excitations of the system, namely, fermionic optical excitations, holon-antiholon pairs, as well as excitons. Our main finding is that the states that dominate the real-time dynamics largely correspond to oscillating $4k_F$ charge and bond instabilities; however, some intermediate states that were observed during the evolution of the system are dominated by the $2k_F$ instability. These results hold for both resonant and nonresonant radiation. We also discuss the relevance of our results to recent experiential findings in organic quasi-1D organic salts.Our numerical results, indicating an ultrafast switching from $2k_F$ to $4k_F$ states, compare well with prior reports that showed a partial or complete melting of the $2k_F$ ground state[12,14].

The outline of the paper is the following: in Sec. II we discuss the Hamiltonian model and the optical excitations relevant to the photoinduced dynamics; Sec. III focuses on the numerical method and procedures used to implement the electric field; in Sec. IV we present the results for the time-dependent behavior of the electronic instabilities and the corresponding analysis; and finally, in Sec. V we close with the conclusions.

II. MODEL AND OPTICAL EXCITATIONS

In this section, we describe the model Hamiltonian used in the study of the light-induced electronic instabilities resulting from the electron-electron and electron-phonon interactions. The electronic degrees of freedom are accounted for using the 1D extended Hubbard Hamiltonian which includes local and nearest-neighbor repulsion between particles. The electron-phonon interaction is incorporated via the Peierls coupling: a dimerization term with a frozen lattice distortion. The phonons are considered to have a much slower dynamics than that of the electrons, i.e., phonons with no dynamics. The resulting extended Peierls-Hubbard (EPH) Hamiltonian[7,22–26] reads

$$H = -\sum_{i,\sigma}\left(t_{i,i+1}\, c^{+}_{i,\sigma}c_{i+1,\sigma} + \text{H.c.}\right) + U\sum_{i} n_{i,\uparrow}n_{i,\downarrow} + V\sum_{i}\left(n_i - n\right)\left(n_{i+1} - n\right), \tag{1}$$

where $t_{i,i+1} = t(1-(-1)^i\delta/2)$ represents the electron-phonon coupling via the dimerization term δ, and t is the electronic hopping between neighboring sites in the absence of the dimerization. The parameters U and V are the local and nearest-neighbor Coulomb repulsion, respectively; the rest of the notation is standard[7,22–26]. The filling is set to quarter filling, $n = 1/2$, and can be interpreted as electrons or holes depending on the specific organic compound under consideration.

Since we are only interested in the electronic properties, we neglect any dynamical terms related to the light and consider it as an external classical field. The interaction with light is incorporated via the minimal coupling, which when using the flux or velocity gauge[27], is expressed in second quantization by an effective flux that modifies the hopping term as $t \rightarrow t\, e^{i\phi/L}$, where L is the system's length. The magnetic flux, ϕ, comes from the oscillating vector potential dependent on time, τ: $\phi = a\, A(\tau)$ with a the lattice constant and where

$$A(\tau) = A_0\, e^{-(\tau-\tau_p)^2/2\sigma^2}\cos\left[\omega_p(\tau-\tau_p)\right], \tag{2}$$

is the explicit form of the vector potential[27]. A_0, ω_p, and σ represent the intensity, frequency, and width of the light pulse and τ_p corresponds to the time when the electric field reaches its maximum value.

We now revisit some of the properties of the EPH model relevant to our study. The EPH model displays a variety of ground states depending on the values of U, V, and δ. Usually, ground and excited states include coexistence of $2k_F$ and $4k_F$ CO, CDW, BOW, SP, and SDW states[22–24,26]. At quarter filling, the ground state is an insulator that is driven by the opening of the dimerization gap $\Delta = 2\delta t$ and the effect of the interactions U and V[25]. In principle, all kinds of combinations of instabilities are possible; however, those that are truly relevant will depend on the type of experiment and material under scrutiny. Different materials properties are driven by

different types of interactions (this is reflected in the values taken by the parameters of the EPH Hamiltonian). Therefore, different competing instabilities will form the excitation spectrum and, accordingly, different states will be sampled in a pump-and-probe experimental setup.

Also important for our purposes are the optical excitations of the EPH model[7]. In the limit of a large dimerization gap, $\delta \lesssim 2$ and $V = 0$, optical excitations will be formed by a pair of fermionic quasi-particles with opposite spin and charge: one hole in the valence band and one electron in the conduction band. Whereas for $V < 2t$ and $\delta < 1$, the optical excitations are made of unbound spinless holon-antiholon pairs: the holon (antiholon) belongs to the lower (upper) Hubbard. For $V > 2t$ and $\delta < 1$, these unbound pairs bond, forming Mott-Hubbard excitons.

In the limit of large dimerization, the optical conductivity has three clear spectral structures. (1) For energies, ω, larger than the dimerization gap, the optical spectrum has contributions from interdimer excitations with peaks at $\omega = 2t(1+\delta/2)$ and $\omega = 2t(1+\delta/2)+U$. These energies correspond to the annihilation of a bonding state in one dimer and the creation of an antibonding state on the neighboring dimer. In particular, $\omega = 2t(1+\delta/2)$ corresponds to the formation of a triplet state on the second dimer giving rise to spin-Peierls coupling. (2) Below the dimerization gap, the optical excitations are those of an effective half-filled Hubbard chain with an absorption band centered around $\omega = U_{\text{eff}} = U/2$. (3) For $\omega = \Delta$, there is a narrow absorption band associated with intradimer excitations of bandwidth proportional to $t(1-\delta/2)$. Most of the optical weight is located at this energy[7].

Increasing interactions and decreasing the dimerization lead to a different structure of the optical spectrum. The optical conductivity is made of one absorption band (a continuum of unbound holon-antiholon pairs) that starts at the Mott gap and has a maximum close to it. The position of the maximum and the onset of the spectral weight depend on the interaction parameters. This maximum will become the Drude peak in the limit $\delta \to 0$; spectral features around $\omega = U$ are also expected and are related to optical excitations from the lower to the upper Hubbard bands[7,28].

As in the case of $U = 0$, the optical gap equals the Mott gap for $V < 2t$. Therefore, the low-energy spectrum still corresponds to unbound pairs of charged excitations. For larger $V > 2t$, the optical gap is smaller than the Mott gap signaling the appearance of an excitonic peak, radically changing the low-energy spectrum[7,28].

The presence of the time-dependent electric field will generate inter- and intradimer excitations, excitons, or holon-antiholon pairs at different characteristic timescales, which are associated with the energy of these excitations, depending on the parameters of the EPH model. Therefore, the understanding of the optical excitations in the system will prove crucial to the understanding of the photoinduced dynamics and concomitant melting of the charge and bond orders. We will see below that the photoinduced dynamics is dominated by the aforementioned optical excitations.

III. METHOD AND PROCEDURES

We now describe the procedure followed in the calculation of the photoinduced dynamics. The ground sate of the EPH model, i.e. for $A = 0$, was calculated using static DMRG[19–21]. Then, using time-dependent DMRG (t-DMRG)[20,21,29,30], we applied the light pulse for a time interval $t_{\text{pump}} = 8\sigma$ with $A(\tau)$ as given in Eq. (2). Once the pulse was applied, the system is subsequently time evolved under H with $A = 0$, i.e., the static EPH model [Eq. (1)], using again t-DMRG. During the entire time evolution, we calculated the time dependence of the mean value of charge, $\langle n_i \rangle$, and the correlations associated with bond $\langle c^+_{i+1} c_i \rangle$, charge $\langle n_{i+1} n_i \rangle$, and spin $\langle S^+_{i+1} S^-_i \rangle$ orders.

In order to calculate the weight of the electronic instabilities from the t-DMRG results, we have performed fittings[31] for each time slice to the following parametrizations of the electronic instabilities[23,26]

$$\begin{aligned} \Delta n_i &= n_{4k_F} \cos(4k_F r_i) + n_{2k_F} \cos(2k_F r_i + \Phi_{2k_F}), \\ b_i &= b_{4k_F} \cos(4k_F r_i) + b_{2k_F} \cos(2k_F r_i + \Phi_{2k_F}), \end{aligned} \tag{3}$$

for charge ($\Delta n_i := n_i - n$), spin, and bond orders; here, $r_i/a = i$, the Fermi wavevector is $k_F = n\pi/2$, and c_{4k_F} and c_{2k_F} characterize the amplitude of the modulations of the $4k_F$ and $2k_F$ excitations ($c = n$ and b for charge and bond orders respectively). A relative phase, Φ_{2k_F}, has been included to account for both states, site- and bond-centered waves[23]. Notice that this phase takes commensurate values when describing different ordered ground states; however, we will see that Φ_{2k_F} can also take incommensurate values for the states that arise from the photostimulation. In order to understand the time-dependent tendency of the photoexcited instabilities, a Fourier transform analysis was performed and compared to the optical excitations.

The reliability of the value of the instabilities coming from the fittings have been cross-checked with calculations of order parameters that are obtained from the time-dependent correlation functions of the bond, charge, and spin orders, namely,

$$\begin{aligned} \langle n^O_{4k_F} \rangle &= \frac{1}{L} \sum_i (-1)^i \langle n_i \rangle, \\ \langle n^O_{2k_F} \rangle &= \frac{1}{L} \sum_i (-1)^{\lfloor i/2 \rfloor} \langle n_i \rangle, \\ \langle b^O \rangle &= \frac{1}{L} \sum_{i,\sigma} \langle c^+_{i+1\sigma} c_{i\sigma} + \text{H.c.} \rangle. \end{aligned} \tag{4}$$

Our static and time-dependent DMRG simulations have been done for several system sizes, $L = 12 - 48$ sites, while up to $m = 400$ states per block were kept

leading to discarded weights of 10^{-6} for the longest time reached. The results shown here correspond to $L = 24$ up to $\tau \approx 90/t$; however, similar τ dependence was observed for $L = 36$ in the same time range, and for $L = 48$ at early times. We notice that the finite-size effects in the EPH model are small for $L \gtrsim 20$, as previously report in Ref. 26. The time step was set to $\tau = 0.05\ [1/t]$, the runs were done up to times $\tau \sim 120\ [1/t]$, and we have used a third-order Suzuki-Trotter expansion of the evolution operator. Open boundary conditions were imposed.

IV. RESULTS

In this section, we will discuss our main results corresponding to the time-dependent photoinduced dynamics of the electronic instabilities in the EPH model, Eq. (1), as obtained with t-DMRG. The particular set of parameters chosen were used in previous dynamical DMRG calculations of the optical conductivity in the EPH model, allowing us to know in advance the main excitation frequencies[7]. First, we will discuss the case of interaction with resonant light, and then we will discuss the regime of a nonresonant intense electromagnetic perturbation.

A. Resonant case

Let us start by analyzing the results shown in Fig. 1, considering the discussion of Sec. III, in the limit of large dimerization. The parameters chosen were $\delta = 1.64$, $U = 3.64t$, $V = 0$[7]; the frequency and amplitude of the electric field were $\omega_p = 4.36t$, $\sigma = 0.7/t$, and $A_0 = 1.75$. In this case the singularities in $\sigma(\omega)$ are square-root divergences and, therefore, clear oscillations are expected in the photodynamics[7,28]. The top plot in Fig. 1, shows the instabilities associated with the charge. At $\tau = 0$, the dominant state is the $2k_F$ instability: $n_{2k_F} \approx 0.001$ and $n_{4k_F} \approx 10^{-7}$. Although n_{2k_F} is small, there is a clear tendency towards this instability when inspecting n_i vs i (not shown). We notice that n_{2k_F} is finite due to the open boundaries; nevertheless, considering such boundaries as scattering impurities, it is interesting to explore its role in the relaxation and effect of the photodynamics of the system. As the system is being pumped, the $4k_F$ instability is greatly enhanced and shows clear oscillations that can be related to the intra-dimer band present in the $\sigma(\omega)$ at $\omega = 2t(1+\delta/2)$. Inter-dimer excitations at the same energy also contribute to the dynamics; as discussed above, this excitation energy, at $\omega = 2t(1+\delta/2)$, is also associated with spin degrees of freedom. The frequency of the oscillations corresponds to energies associated with the edges and center of this band. An overall decay of n_{4k_F} and a slight increase of n_{2k_F} is observed as time advances, eventually leading to an asymptotic state which resembles the original ground state.

The bottom plot in Fig. 1 shows the time evolution of the bond instabilities in the large dimerization limit.

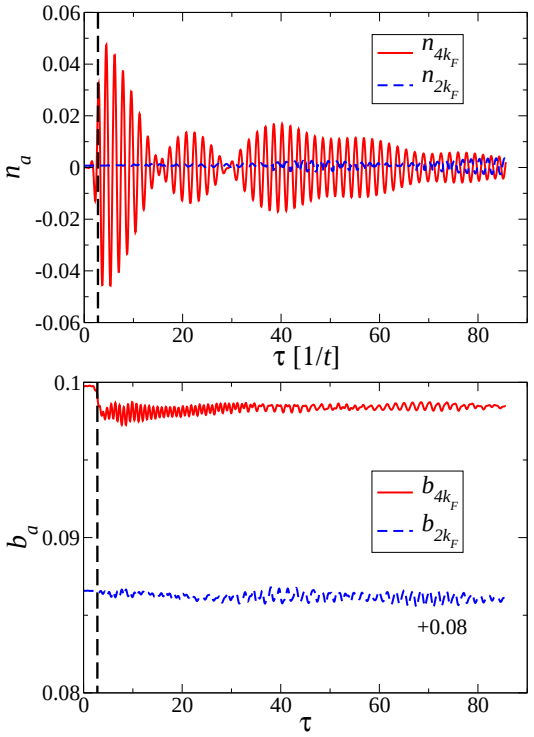

FIG. 1. Photoexcited time evolution of the charge (top) and bond (bottom) instabilities, $a = 2k_F$ and $4k_F$, in the large dimerization limit. The vertical dashed line corresponds to the maximum amplitude of the resonant light at τ_p and parameters: $\delta = 1.64$, $U = 3.64t$, $V = 0$, $A_0 = 1.75$, $\omega_p = 4.36t$, $\sigma = 0.7/t$.

For $\tau = 0$, the ground state possesses an SP coupling, as corroborated by the quantities $\langle S^+_{i+1} S^-_i \rangle$ and $\langle b^O \rangle$ calculated with static DMRG, with contributions from both $2k_F$ and $4k_F$ instabilities. After the system is pumped, we see a decrease in b_{4k_F} and a subsequent recovery. The small changes in the bond order can be related to the existence of strong dimers due to the large value of δ. At early times the frequency of oscillations corresponds to the energy $\omega = 2t(1+\delta/2) + U$; on the other hand, b_{2k_F} alternates with a frequency $\omega = 2t(1+\delta/2)$ which is the energy of the formation of the triplet state, signaling the presence of the SP state. A spectral analysis (not shown)[32] also shows the generation of holon-antiholon pairs at approximately the energy $\omega = U_{\rm eff}/2$ related to the effective Hubbard chain (see Sec. II).

Decreasing δ and increasing U leads to a square-root onset of spectral weight at the optical gap as the main feature in $\sigma(\omega)$[7,28]. Therefore, in this case we do not expect sharp oscillations due to the lack of resonances (singularities). That is why we have set ω_p to the maximum that appears after the onset of spectral weight. Figure 2 shows the photodynamics for the case $\delta = 0.35$, $U = 8.24t$, $V = 1.64t$[7]; the electric field parameters are $A_0 = 2.75$, $\omega_p = 0.81t$, $\sigma = 3/t$. For this set of parameters the ground state corresponds to a $2k_F$ CDW with $\ldots 1100 \ldots$ CO plus a $2k_F$ and $4k_F$ BOW state[22,26]. The

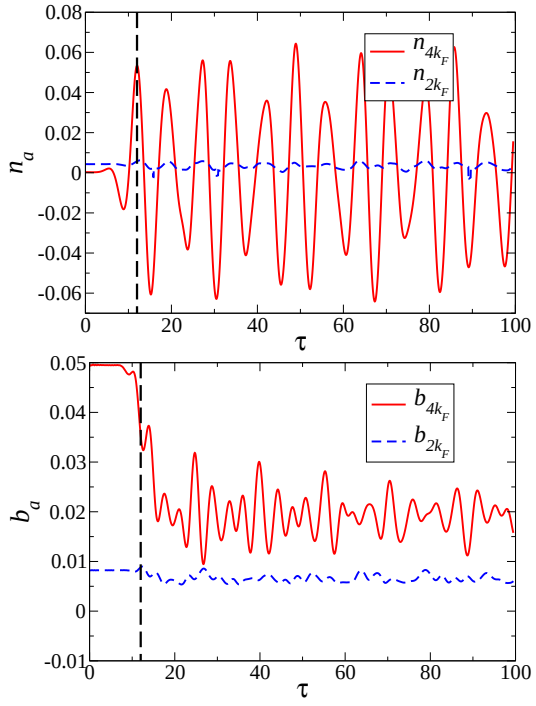

FIG. 2. Photoexcited time evolution of the charge (top) and bond (bottom) instabilities, $a = 2k_F$ and $4k_F$. The vertical dashed line corresponds to the maximum amplitude of the resonant light at τ_p and parameters: $\delta = 0.35$, $U = 8.24t$, $V = 1.64t$, $A_0 = 2.75$, $\omega_p = 0.81t$, $\sigma = 3/t$.

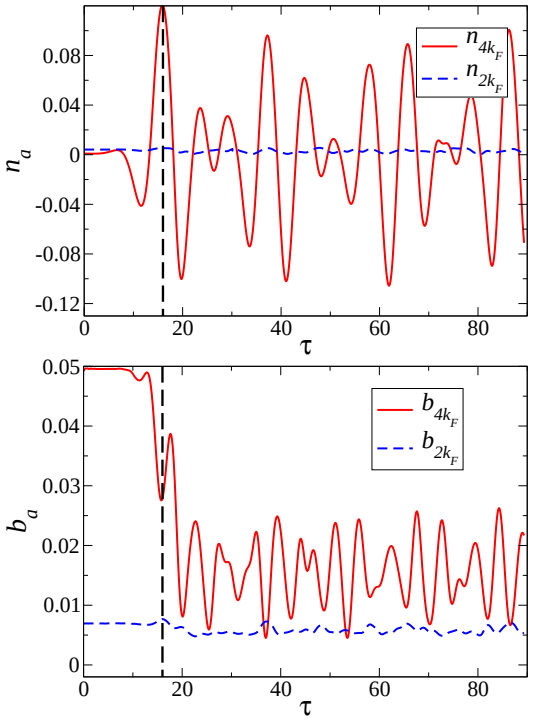

FIG. 3. Photoexcited time evolution of the charge (top) and bond (bottom) instabilities, $a = 2k_F$ and $4k_F$. The vertical dashed line corresponds to the maximum amplitude of the resonant light at τ_p and parameters: $\delta = 0.35$, $U = 8.24t$, $V = 3.29t$, $A_0 = 3.75$, $\omega_p = 0.55t$, $\sigma = 4/t$.

charge instabilities (top plot, Fig. 2) display oscillations that can be associated with energies close to the edge of the optical absorption spectrum set by the Mott gap $\omega \sim E_c = 0.95t$. As the electric field pumps the system, n_{2k_F} gets reduced whereas n_{4k_F} is enhanced; and as time evolves, only n_{4k_F} contributes to the overall dynamics. Notice that the apparent on-phase behavior of n_{2k_F} and n_{4k_F} is corrected by the presence of the phase Φ_{2k_F}, which oscillates nontrivially (not shown).

As for the time-dependent behavior of the bond instabilities (Fig. 2, bottom), both b_{4k_F} and b_{2k_F} are reduced as the system is excited by the external radiation. The enhanced reduction in b_{4k_F} can be attributed to a strong coupling between the current operator and states with a unit cell of two sites. The characteristic frequencies have the same physical nature as in the case of the charge; i.e., they belong to unbound optical excitations. Similar results for the photodynamics are found for the case $V = 0$ (not shown). This type of trend in the evolution of the electronic instabilities is expected to be valid for $V < 2t$, where no bound excitations (excitons) are created.

As discussed in Sec. II, for $V > 2t$, the presence of excitons radically modify the spectral properties[7,28]. A well-defined resonance (a delta peak) at the optical gap leads to sharp oscillations in the instabilities as a function of time. Figure 3 shows the oscillations of the electronic instabilities for the case $\delta = 0.35$, $U = 8.24t$, $V = 3.29t$[7], and electric field parameters $A_0 = 3.75$, $\omega_p = 0.55t$, $\sigma = 4/t$, where the presence of excitons has been shown before[7]. The evolution in time of n_{4k_F} (Fig. 3, top) shows an abrupt increase as the system is pumped, reaching its maximum around the radiation pulse maximum; whereas n_{2k_F} is fairly insensitive to the radiation. Interestingly, the charge oscillation is related to the bound energy of the exciton $E_b = 0.9t$ and the excitonic energy that equals the optical gap. The characteristic frequency comes from resonance between the excitonic peak at $\omega = 0.55t$ and the onset of the absorption band of holon-antiholon pairs ($E_c = 1.4t$).

The bond instabilities are shown in the bottom panel of Fig. 3. Similarly to the case of charge, in this case the photodynamics is dominated by b_{4k_F} while b_{2k_F} remains slightly unaffected, at least in the time domain studied. Similarly as in the situation in the previous figures, once the electric field reaches its maximum, b_{4k_F} is considerably reduced and, at later times, there is a small recovery of the bond instability accompanied by oscillations related to the bound energy of the exciton.

We conclude this section noticing that the oscillations of the photogenerated dynamics are greatly modified by the optical excitations and by whether these excitations are true singularities or not. It is also important to notice that the phase Φ_{2k_F}/π takes oscillatory incommensurate values (not shown), giving rise to states that differ from the ground state situation where Φ_{2k_F}/π can only take

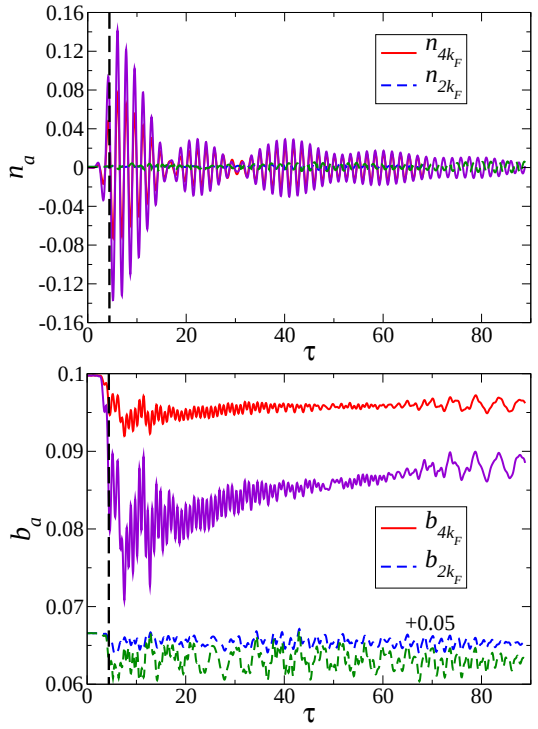

FIG. 4. Photoexcited time-evolution of the charge (top) and bond (bottom) instabilities, $a = 2k_F$ and $4k_F$, in the large dimerization limit. The vertical dashed line corresponds to the maximum amplitude of the nonresonant light at τ_p and parameters: $\delta = 1.64$, $U = 3.64t$, $V = 0$, $A_0 = 3.5$ (red and blue) and 7 (violet and green), $\omega_p = 2.5t$, $\sigma = 1.1/t$.

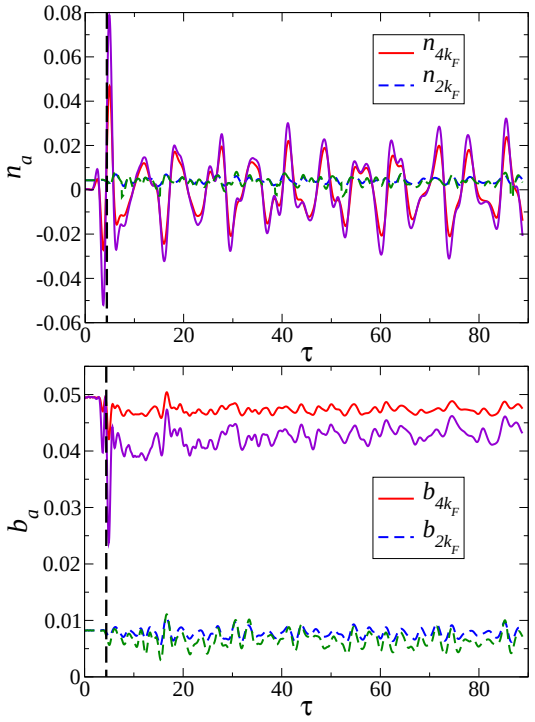

FIG. 5. Photoexcited time-evolution of the charge (top) and bond (bottom) instabilities, $a = 2k_F$ and $4k_F$. The vertical dashed line corresponds to the maximum amplitude of the nonresonant light at τ_p and parameters: $\delta = 0.35$, $U = 8.24t$, $V = 1.64t$, $A_0 = 5.5$ (red and blue) and 11 (violet and green), $\omega_p = 2.5t$, $\sigma = 1.1/t$.

commensurate values. Notice that these states can be associated with nonthermal states observed in spectroscopy experiments[5,6].

B. Nonresonant case

In this section we will explore the effects of a nonresonant intense electric field which takes advantage of the ponderomotive effect. It is expected that this effect will give rise to similar results as in the resonant case. All the results shown in this section were done using a frequency of the electric field $\omega_p = 2.5t$, $\tau_p = 4.4/t$, and $\sigma = 1.1/t$; we notice that this value does not match any optical excitations[7]. We also used the same parameters in the EPH model as in the resonant case so we can make a direct comparison with the nonresonant situation.

The photoinduced dynamics of the charge is shown in the top panel of Fig. 4 for two different values of the amplitude of the incident radiation ($A_0 = 3.5$ and 7) and parameters $\delta = 1.64$, $U = 3.64t$, $V = 0$. After the system is pumped, n_{4k_F} oscillates with the same frequency as in the resonant case (see Fig. 1); i.e., intra- and interdimer excitations of energy $\omega = 2t(1 + \delta/2)$ dictate its time-dependent dynamics. The oscillations are accompanied by a decay in the amplitude as time evolves. The n_{2k_F} instability, on the other hand, remains largely unaffected by the pulse in the time window explored. At later times there is a decay in the amplitude of the oscillations of the charge.

The nonresonant response of the bond instabilities, shown in Fig. 4 (bottom panel), are also quite similar to the resonant case. Not only intra- and interdimer excitations, but also the low-energy absorption band of the spectrum ($\omega < 2\Delta$) contribute to the photodynamics. Notice that in contrast with the charge case, the amplitude of the oscillations of b_{4k_F} and b_{2k_F} are differently affected by different amplitudes of the electric field, leading to different decaying rates for different values of A_0. Nevertheless, the frequency of the excitations are unaffected by the amplitude of the external radiation; this is a feature of nonresonant photodynamics.

Figure 5 displays the dynamics of the electronic instabilities for the case $\delta = 0.35$, $U = 8.24t$, and $V = 1.64t$, with amplitudes of the electric field $A_0 = 5.5$ and 11. In the case of charge instabilities, regardless of the intensity of the laser light, n_{2k_F} is barely affected, contrary to n_{4k_F} (Fig. 5, top). At time $\tau = \tau_p$, the $4k_F$ order is largely enhanced with a posterior reduction in the oscillation amplitude. A Fourier analysis (not shown here) revealed that the band of frequencies of the oscillations has a wider spectral range and smaller weights than in

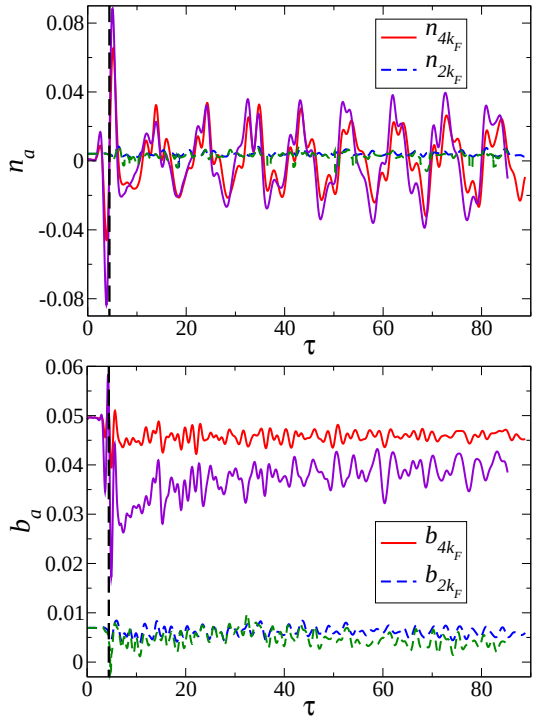

FIG. 6. Photoexcited time-evolution of the charge (top) and bond (bottom) instabilities, $a = 2k_F$ and $4k_F$. The vertical dashed line corresponds to the maximum amplitude of the nonresonant light at τ_p and parameters: $\delta = 0.35$, $U = 8.24t$, $V = 3.29t$, $A_0 = 7.5$ (red and blue) and 15 (violet and green), $\omega_p = 2.5t$, $\sigma = 1.1/t$.

the resonant case (see Fig. 2). The characteristic energies associated with these frequencies are related with those of holon-antiholon pairs.

The time evolution of the bond order for the same parameters is shown in the bottom panel of Fig. 5. At time $\tau = \tau_p$, the $4k_F$ order is greatly reduced and then quickly restored (although not completely) followed by weak oscillations. On the other hand, b_{2k_F} is only moderately affected by the pulse intensity around $\tau = \tau_p$; nevertheless, the field does create oscillations at later times similar to those of b_{4k_F}. The physical character of the oscillations is the same as for the charge instabilities.

The presence of excitons as the low-energy optical excitation is explored for the parameters $\delta = 0.35$, $U = 8.24t$, $V = 3.29t$, with electric field amplitudes $A_0 = 7.5$ and 15. The behavior of the electronic instabilities does not change the system response to an intense light pulse around $\tau = \tau_p$ compared to the case shown in Fig. 5; however, the origin of the oscillations is quite different, as explained below. The time evolution of the charge and bond instabilities, shown in the top and bottom panels of Fig. 6, respectively, display similar behaviors to those in the case shown in Fig. 3. n_{4k_F} increases as the pulse reaches its maximal value at $\tau = \tau_p$, and once the pulse is applied, n_{4k_F} decreases and starts oscillating with a smaller amplitude. n_{2k_F} is slightly affected in the time window considered. The nature of the oscillations can be attributed to the photogeneration of excitonic energy and the band of unbound pairs, just as in the case shown in Fig. 3.

The effect of the electric field on b_{4k_F} and b_{2k_F} is shown in the bottom panel of Fig. 6. At early times these instabilities are significantly reduced; this effect is stronger for the $4k_F$ instability. For times $\tau > t_{\rm pump}$, b_{2k_F} quickly relaxes back to its original value at $\tau = 0$; this quick recovery is followed by clear oscillations. On the other hand, b_{4k_F} displays a slower relaxation rate than b_{2k_F} without reaching its original value. As in the case of the charge instability, the oscillations are associated with the energies of bound (excitons) and unbound (holon-antiholon pairs) optical excitations; the long-time physics of the photodynamics is again closely related to that of the resonant case.

C. Discussion

Assuming that the static phase diagram has the same states, although redistributed, as the nonstatic phase diagram, then interesting features appear. For instance, notice that when $n_{4k_F} = 0$ for finite τ, the system closely resembles the ground state ($\tau = 0$); however, the values of b_{4k_F} and b_{2k_F} do not correspond to those of the ground state. Since we are studying a closed system, the electric field will pump energy into it, and it is expected that the long time behavior will be described by a thermal distribution. However, it is possible to assign effective interaction parameters to these time-dependent states that are closely related to the original parameters in the phase diagram; in other words, one can envision each finite-τ state as a ground state of a Hamiltonian with parameters which depend on time. On the other hand, if we focus on the extreme values of n_{4k_F}, the effective parameters that we can assign to the time-dependent state will be farther away, in the phase diagram, from the original ones. This situation implies a vast sampling of the phase space through photoirradiation; whether this sampling is bounded or not remains as an open question. The above argument holds in general and does not depend on the parameters or the nature of the radiation.

The main difference between resonant and nonresonant pumping lies in how the system behaves around $\tau = \tau_p$ and the amplitude of the resulting oscillations. The general trend is that the charge instabilities, in the nonresonant case, will oscillate with a wider range of frequencies and lower amplitudes than in the resonant scenario, at least for $\tau > t_{\rm pump}$. For the bond instabilities, the system always shows a degree of relaxation after the photoexcitation and a considerable reduction of its value around $\tau = \tau_p$. In the resonant case, the photoinduced changes and oscillations of the instabilities are robust (the amplitude of the oscillations remains stable in the entire time window); whereas in the nonresonant case the electronic instabilities are greatly modified around $\tau = t_{\rm pump}$ fol-

lowed by a still visible, albeit smaller, change in the amplitude of the oscillations.

This is in accord with the ponderomotive effect which comes into play when an off-resonant electric field is applied to the system[4,33,34]. Indeed, there is a process which is not instantaneous and is inherent to the off-resonant response of the system to the accumulation of energy associated with the ponderomotive effect, that goes as A_0^2. After such energy has been absorbed, the system is capable of creating optical excitations displaying the consequent oscillatory behavior with the characteristic frequencies of those excitations. The observed delay, at times $\tau \gtrsim \tau_p$, in the creation of these excitations will depend on the energy associated with such excitations, ω, and the amplitude of the electromagnetic pulse, A_0.

Notice also that the response of the charge order to different electric field amplitudes is different from that of the bond order. As expected from the ponderomotive effect, at earlier times $\tau \sim \tau_p$ both charge and bond instabilities have dynamics with similar frequencies but different amplitudes; however, for longer times, $\tau > t_{\rm pump}$, the charge excitations have similar amplitudes regardless of the value of A_0, whereas the bond instability clearly shows different amplitudes in its photodynamics for different values of A_0. The different dependence of the photodynamics on A_0, for charge and bond instabilities, remains in the way the energy accumulated is distributed along charge and bond excitations.

A general result from this study is that the 1D EPH model for charge-transfer systems, with no phonon dynamics, will tend to largely enhance the $4k_F$ charge instability and that this electronic instability fluctuates between (0101) and (1010) states. The time-dependent dynamics of the electronic instabilities shows the photoinduced melting of the $2k_F$ charge state and the concomitant replacement by the $4k_F$ ordered state. This ensuing dynamics is mediated by the photogeneration of optical excitations. On the other hand, the $2k_F$ bond and charge instabilities are not greatly affected by the presence of the electric field. We believe that the $4k_F$ instability is considerably more sensitive than the $2k_F$ instability to the excitation with light, probably due to the fact that the current operator, or equivalently the kinetic energy operator, only strongly couples $4k_F$ states (i.e., neighboring sites). We speculate that if one considers longer-range hopping, the $2k_F$ states will be largely affected by the time-dependent electric field.

Regardless of the nature of the light interacting with the system, this scenario is observed in the photogenerated dynamics for all of the parameters studied in this work. Changing the parameters will only affect the characteristic frequencies, and at a minor level, the amplitude of the oscillations of the instabilities; in other words, the main role that the optical excitations (holon-antiholon pairs, excitons, etc.) play in the photodynamics is setting the frequency of the charge and bond oscillations.

The results presented in this work could have potential applications in the optoelectronics of charge-transfer systems. Taking advantage of the enormous positive/negative oscillating response of the $4k_F$ instability, organic charge-transfer systems can be used as switching devices with femtosecond response (provided that in such systems the vibrational degrees of freedom are slow compared to any other electronic time scale)[5,6].

V. CONCLUSION

In this publication, we have investigated the time-dependent behavior of the photoexcited electronic instabilities of a quarter-filled one-dimensional extended Peierls-Hubbard model, using static and time-dependent DMRG methods. Both charge and bond instabilities were studied as a function of time when the system is pumped with a resonant or nonresonant few-cycle electric field. Their resulting behavior can be explained in the light of the system optical excitations. Our main results show that the overall dynamics of the $4k_F$ bond and charge instabilities corresponds to a gigantic fluctuating behavior as a function of time. By contrast, the time-dependent response of the $2k_F$ instability (both for bond and charge) to the incident radiation displays a fairly smooth trend. These results remain valid whether the applied light pulse is in or off resonance with the optical excitations of the system, and regardless of the nature of such excitations. We argue that our calculations indicate that charge-transfer organic systems with slow phonon dynamics will display robust switching properties that can be potentially used in optoelectronic devices.

ACKNOWLEDGMENTS

J.R. acknowledges G. B. Martins for insightful conversations. Support by the Early Career Research Program, Scientific User Facilities Division, Basic Energy Sciences, US Department of Energy, under contract with UT-Battelle (J.R., K.A.) is acknowledged. A.E.F. was supported by the National Science Foundation through grant DMR-1339564 and E.D. through grant DMR-1404375.

[1] P. B. Corkum and F. Krausz, *Nat. Phys.* **3**, 381 (2007).
[2] E. Goulielmakis, V. S. Yakovlev, A. L. Cavalieri, M. Uiberacker, V. Pervak, A. Apolonski, R. Kienberger, U. Kleineberg, F. Krausz, *Science 317*, 769 (2007).
[3] J. Orenstein, *Physics Today* **65**, 44 (2012).
[4] T. Kampfrath, K. Tanaka, and K. A. Nelson, *Nature Photon.* **7**, 680 (2013).

[5] M. Chollet, L. Guerin, Na. Uchida, S. Fukaya, H. Shimoda, T. Ishikawa, K. Matsuda, T. Hasegawa, A. Ota, H. Yamochi, G. Saito, R. Tazaki, S.-I. Adachi, S.-Y. Koshihara, *Science* **307**, 86 (2005).

[6] K. Onda, S. Ogihara, K. Yonemitsu, N. Maeshima, T. Ishikawa, Y. Okimoto, X. Shao, Y. Nakano, H. Yamochi, G. Saito, and S.-Y. Koshihara, *Phys. Rev. Lett.* **101**, 067403 (2008).

[7] H. Benthien and E. Jeckelmann, *Eur. Phys. J. B* **44**, 287 (2005).

[8] H. Okamoto, H. Matsuzaki, T. Wakabayashi, Y. Takahashi, and T. Hasegawa *Phys. Rev. Lett.* **98**, 037401 (2007).

[9] N. Maeshima and K. Yonemitsu, *J. Phys. Soc. Jpn.* **74**, 2671 (2005).

[10] N. Maeshima and K. Yonemitsu, *Phys. Rev. B* **74**, 155105 (2006).

[11] N. Maeshima and K. Yonemitsu, *J. Phys. Soc. Jpn.* **76**, 074713 (2007).

[12] K. Yonemitsu and N. Maeshima, *Phys. Rev. B* **76**, 075105 (2007).

[13] K. Yonemitsu and N. Maeshima, Y. Tanaka, and S. Miyashita, *J. Phys.: Conf. Ser.* **148**, 012054 (2009).

[14] J. D. Lee, *Phys. Rev. B* **80**, 165101 (2009).

[15] K. Moriya, N. Maeshima and K. I. Hino, *Eur. Phys. J. B* **85**, 350 (2012).

[16] H. Uemura, N. Maeshima, K. Yonemitsu, H. Okamoto, *Phys. Rev. B* **85**, 125112 (2012).

[17] H. Lu, S. Sota, H. Matsueda, J. Bonča, and T. Tohyama, *Phys. Rev. Lett.* **109**, 197401 (2012),

[18] H. Matsueda, S. Sota, T. Tohyama, and S. Maekawa, *J. Phys. Soc. Jpn.* **81**, 013701 (2012).

[19] S. R. White, *Phys. Rev. Lett.* **69**, 2863 (1992); *ibid.*, *Phys. Rev. B* **48**, 10345 (1993).

[20] U. Schollwöck, *Rev. Mod. Phys.* **77**, 259 (2005).

[21] K. Hallberg, *Adv. Phys.* **55**, 477 (2006).

[22] K. C. Ung, S. Mazumdar, and D. Toussaint, *Phys. Rev. Lett.* **73**, 2603 (1994).

[23] J. Riera and D. Poilblanc, *Phys. Rev. B* **65**, 16243(R) (2000).

[24] Y. Shibata, S. Nishimoto, and Y. Ohta, *Phys. Rev. B* **64**, 235107 (2001).

[25] M. Tsuchiizu, H. Yoshioka, and Y. Suzumura, *J. Phys. Soc. Jpn.* **70**, 1460 (2001).

[26] M. Kuwabara, H. Seo, and M. Ogata, *J. Phys. Soc. Jpn.* **72**, 225 (2003).

[27] L. B. Madsen, *Phys. Rev. A* **65**, 053417 (2002).

[28] E. Jeckelmann, *Phys. Rev. B* **67**, 075106 (2003).

[29] S. R. White and A. E. Feiguin, *Phys. Rev. Lett.* **93**, 076401 (2004).

[30] A. J. Daley, C. Kollath, U. Schollwöck and G. Vidal, J. Stat. Mech.: Theor. Exp. **P04005** (2004).

[31] The fittings have been performed in an $L/2$-site segment which is centered in the middle of the full L-site system to try to avoid Friedel oscillations introduced by the open boundaries. Some peaked behavior of the instabilities is observed due to convergence issues of the highly nonlinear fittings.

[32] The energies obtained by a Fourier decomposition of the τ-dependent instabilities were associated to the optical excitacions.

[33] H. Wen, M. Wiczer, and A. M. Lindenberg, *Phys. Rev. B* **78**, 125203 (2008).

[34] H. Hirori, K. Shinokita, M. Shirai, S. Tani, Y. Kadoya, and K. Tanaka, *Nat. Comm.* **2**, 594 (2011).